



Origin of the reduced exchange bias in an epitaxial FeNi(111)/CoO(111) bilayer

F. Radu,* S. K. Mishra, I. Zizak, A. I. Erko, H. A. Dürr, and W. Eberhardt

Helmholtz-Zentrum Berlin für Materialien und Energie, Albert-Einstein Strasse 15, D-12489 Berlin, Germany

G. Nowak, S. Buschhorn, and H. Zabel

Institut für Experimentalphysik/Festkörperphysik, Ruhr-Universität Bochum, D-44780 Bochum, Germany

K. Zhernenkov and M. Wolff

*Institut für Experimentalphysik/Festkörperphysik, Ruhr-Universität Bochum, D-44780 Bochum, Germany
and Institut Laue-Langevin, F-38042 Grenoble Cedex 9, France*

D. Schmitz, E. Schierle, E. Dudzik, and R. Feyerherm

Helmholtz-Zentrum Berlin für Materialien und Energie, Glienicker Str. 100, D-14109 Berlin, Germany

(Received 3 August 2008; revised manuscript received 7 April 2009; published 21 May 2009)

We have employed soft and hard x-ray resonant magnetic scattering and polarized neutron diffraction to study the magnetic interface and the bulk antiferromagnetic domain state of the archetypal epitaxial Ni₈₁Fe₁₉(111)/CoO(111) exchange biased bilayer. The combination of these scattering methods provides unprecedented detailed insights into the still incomplete understanding of some key manifestations of the exchange bias effect. We show that the several orders of magnitude difference between the expected and measured value of exchange bias field is caused by an anisotropic in-plane orientation of antiferromagnetic domains. Irreversible changes in their configuration lead to a training effect. This is directly seen as a change in the magnetic half-order Bragg peaks after magnetization reversal. The antiferromagnetic domain size is extracted from the width of the $(\frac{1}{2}\frac{1}{2}\frac{1}{2})$ antiferromagnetic peak by both neutron and x-ray scattering and is determined to be 30 nm in size. A reduced blocking temperature as compared to the measured antiferromagnetic ordering temperature clearly corresponds to the blocking of antiferromagnetic domains. Moreover, an excellent correlation between the size of the antiferromagnetic domains, exchange bias field, and frozen-in spin ratio is found, providing a comprehensive understanding of the origin of exchange bias in epitaxial systems.

DOI: [10.1103/PhysRevB.79.184425](https://doi.org/10.1103/PhysRevB.79.184425)

PACS number(s): 75.60.Jk, 75.70.Cn

I. INTRODUCTION

Although the first exchange biased system was engineered by nature a few billion years ago,¹ its observation has been possible only 60 years ago by Meiklejohn and Bean (M&B) (Ref. 2) when studying Co particles embedded in their natural oxide (CoO) matrix. After the discovery of the giant magnetoresistance (GMR) effect,^{3,4} the exchange bias (EB) effect has become an integral part of modern magnetism with implications for basic research and for numerous device applications such as magnetoelectronic switching devices (spin valves) and for random access magnetic storage units. For these applications a predictable, robust, and tunable exchange bias effect is required.

The EB effect manifests itself in a shift of the hysteresis loop in the negative or the positive direction with respect to the applied field. Its origin is related to the magnetic coupling across the common interface shared by a ferromagnetic (FM) and an antiferromagnetic (AF) layer. Extensive research is being carried out to unveil the microscopic origin of this effect.^{5–10} The details of the EB effect depend crucially on the AF and on the interface separating it from the FM layer. However, some characteristic features are still under debate: (1) the size of the exchange field is up to several orders of magnitude lower than expected for many epitaxial systems with an uncompensated AF surface; (2) exchange bias field (H_{EB}) and coercive field (H_c) increase as the sys-

tem is cooled in an applied magnetic field below the blocking temperature (T_B) of the AF layer with $T_B \leq T_N$, where T_N is the Néel temperature of the AF layer; (3) the magnetization reversal can be different for the ascending and descending part of the hysteresis loop;^{11–16} (4) H_{EB} and H_c can vary when hysteresis loops are measured consecutively, a phenomenon called training effect.¹⁷ Furthermore, a positive H_{EB} has been observed after cooling an AF/FM system in very high magnetic fields at low temperatures^{18,19} and close to the blocking temperature.^{20–22} A considerable number of theoretical models have been developed for describing possible mechanisms of the EB effect. The main motivation for most of them is to describe the discrepancy between the measured versus predicted value for the H_{EB} and H_c .

We address this discrepancy by studying an epitaxial Ni₈₁Fe₁₉(111)/CoO(111) exchange biased bilayer by polarized neutron and x-ray scattering and reflectivity. We show that the exchange bias for an epitaxial Ni₈₁Fe₁₉/CoO is several orders of magnitude less than expected due to the particular domain state of the AF layer. The available coupling energy is transformed in coercivity, mediated by the magnetically disordered interface. The blocking temperature of the exchange bias appears as the blocking of the AF domains, as revealed by neutron scattering. The temperature behavior of the frozen-in and rotatable AF spins is compared to the EB field and average domain sizes.

II. SAMPLE GROWTH AND CHARACTERIZATION

The samples have been grown by dc-magnetron sputtering (at BESSY) in an argon atmosphere of 1.5×10^{-3} mbar with a base pressure of 2×10^{-8} mbar. Unlike the previously grown CoO layers, where rf sputtering was preferred due to the insulating nature of the CoO target, dc-magnetron sputtering offers the advantage of higher deposition rates and, therefore a thicker CoO layer can be grown in stable conditions. Five substrate crystals have been used to test the quality of the CoO films: MgO(100), MgO(110), MgO(111), Al₂O₃(0001), and Al₂O₃(11 $\bar{2}$ 0). Although the last three substrates provide the (111) uncompensated surface for CoO, the highest structural quality was achieved by using an Al₂O₃(11 $\bar{2}$ 0) crystal. The substrate was rinsed in ethanol and cleaned in an ultrasonic bath for 30 min. After annealing to 700 °C for 15 min, the temperature was decreased to 500 °C where a 2000 Å thick CoO layer was grown. Afterward, the temperature was further decreased to room temperature for the deposition of a 120 Å Ni₈₁Fe₁₉ (Permalloy \equiv Py) film. To prevent oxidation, a 50 Å Au capping layer was grown on top of the bilayer. The reduced deposition temperature for the Py and Au layers was chosen in order to reduce temperature induced interdiffusion at the interface.

The structural quality of the samples was studied by using x-ray scattering at the MAGS (Ref. 23) and KMC2 (Ref. 24) x-ray beamlines at BESSY [Figs. 1(a) and 1(b), respectively] using $\lambda=1.5405$ Å. Preliminary diffraction measurements were done in the BESSY Crystallography Laboratory at the two-crystal x-ray diffractometer TRS-1. A longitudinal Bragg scan is shown in Fig. 1(a). The CoO peak at $Q=2.549$ Å⁻¹ occurs at the tabulated value suggesting a stoichiometric growth.²⁵ The Py peak at $Q=3.07$ Å⁻¹ exhibits Laue oscillations which are indicative of an excellent smoothness of the Py/CoO interface. Even the Au capping layer peak at $Q=2.67$ Å⁻¹ exhibits two Laue oscillations, one at $Q=2.77$ Å⁻¹ and another one at $Q=2.57$ Å⁻¹, below the CoO peak. In order to probe the epitaxy relations between the layers we have measured azimuthal scans around the [100] crystallographic orientation, which makes an angle of 35.26° with respect to the sample surface. Sixfold symmetry indicates that the CoO layers consist of at least two crystallographic domains²⁶ rotated 60° with respect to each other. The epitaxial relation extracted from these data can be expressed as CoO[1 $\bar{1}$ 0]||Py[1 $\bar{1}$ 0]||Au[1 $\bar{1}$ 0] and corresponds to the Nishiyama-Wassermann epitaxial growth.^{25,27}

III. OBSERVATION OF ANTIFERROMAGNETIC DOMAINS BY RESONANT X-RAY MAGNETIC SCATTERING

The domain formation in the AF CoO layer was studied using x-ray magnetic scattering at the Co K edge. Measurements were done at the 7 T multipole wiggler beamline MAGS operated by the Helmholtz-Zentrum Berlin at the synchrotron source BESSY II.²³ The sample was cooled from 300 to 10 K in 800 Oe magnetic field applied parallel to the sample surface. The peak shapes of the structural (111) and the AF ($\frac{1}{2}\frac{1}{2}\frac{1}{2}$) Bragg peaks were measured both in the

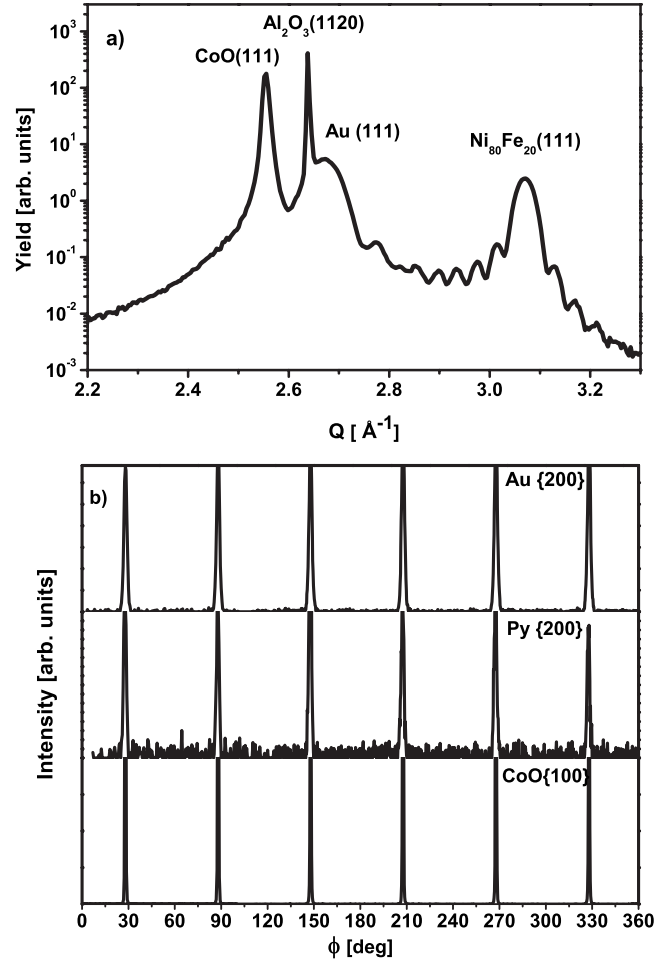


FIG. 1. (a) Longitudinal x-ray diffraction along the [111] crystallographic axes. All layers exhibit a Bragg peak. The Py and Au layers show Laue oscillations suggesting an exceptionally smooth CoO/Py interface. (b) Orientation distribution of [100] plane normals measured by using asymmetric x-ray diffraction. The epitaxial relation between the CoO, Py, and Au layers is CoO[1 $\bar{1}$ 0]||Py[1 $\bar{1}$ 0]||Au[1 $\bar{1}$ 0]. All diffractograms were recorded at $E=8048$ eV ($\lambda=1.5405$ Å).

($\theta/2\theta$) and the transverse (θ rocking scan) geometries. Linear polarization analysis with Au(111) crystal was used to separate structural and magnetic contributions.

Comparing the structural to the magnetic longitudinal peaks [Fig. 2(a) versus Fig. 2(c)] we observe an increase in the full width at half maximum (FWHM) from 0.011 Å⁻¹ to 0.013 Å⁻¹, respectively. The width of the magnetic peak ($\frac{1}{2}\frac{1}{2}\frac{1}{2}$) becomes wider as compared to the structural one (111) suggesting formation of AF domains. Scattering at the magnetic inhomogeneities provided by the domain walls will diminish the average coherence length, providing an increased width of the longitudinal ($\frac{1}{2}\frac{1}{2}\frac{1}{2}$) magnetic peak with respect to its (111) charge scattering counterpart.

The transverse scan shown in Fig. 2(d) probes the in-plane average size of AF domains, often identified as the magnetic coherence length ($L_{AF}=2\pi/\text{FWHM}$).^{28,29} An almost Lorentzian-shaped transverse scan [Fig. 2(d)] is indicative for a broad distribution of domain sizes with a mean

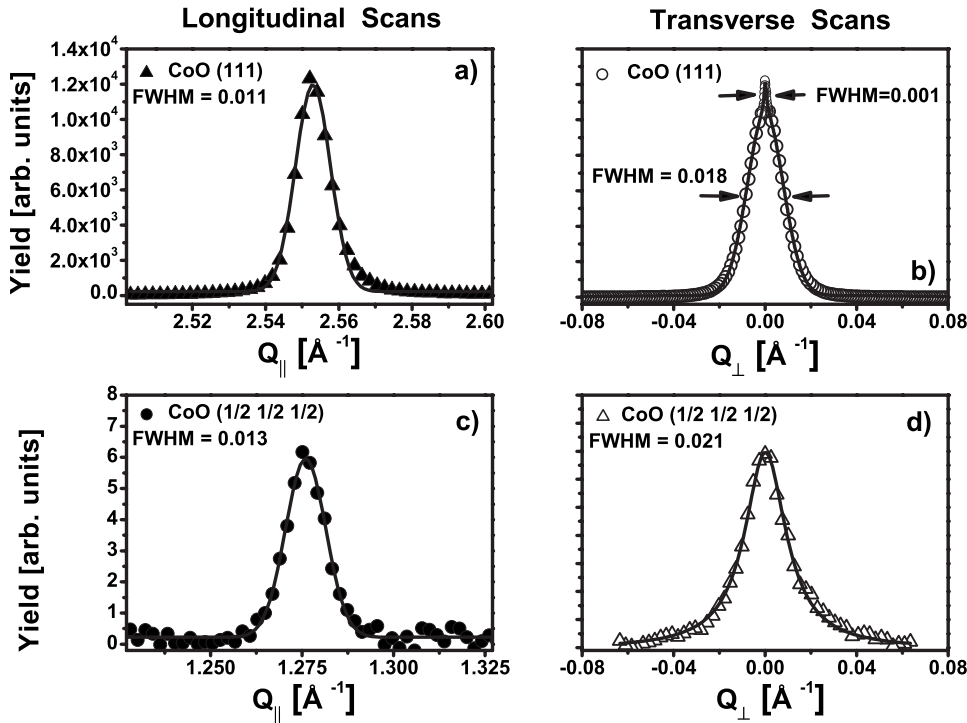


FIG. 2. Resonant x-ray magnetic scattering at the Co K edge: (a) longitudinal and (b) transverse (111) Bragg peaks; (c) longitudinal and (d) transverse $(\frac{1}{2} \frac{1}{2} \frac{1}{2})$ Bragg peaks. The structural (111) peaks provide information about in-plane and out-of-plane charge correlations. The longitudinal and transversal half-order peaks are wider as compared to charge scattering suggesting the formation of AF domains. The width of the magnetic transverse scan provides the in-plane magnetic coherence length for the AF domains. The scans have been measured at 10 K after cooling the sample from above room temperature in an external magnetic field.

value of $L_{AF} \approx 30$ nm. The widths are free of instrumental resolution. Its shape is also quite different from the structural (111) transverse scan [Fig. 2(b)]. A sharp coherent contribution is clearly visible on top of a much broader diffuse peak. The presence of the sharp peak confirms a high-film quality but random vacancies and stacking faults contribute to the broad diffuse charge scattering which becomes more prominent as the film grows thicker.³⁰ Notice that the correlation lengths for both structural and magnetic peaks are very close in magnitude suggesting that the AF domain size is only slightly smaller as compared to the grain size.

IV. MAGNETIZATION REVERSAL AND THE ANTIFERROMAGNETIC DOMAIN STATE BY POLARIZED NEUTRON REFLECTIVITY AND POLARIZED NEUTRON DIFFRACTION

Having established the existence of AF domains in the AF layer, we study now their average in-plane orientation using neutrons. Polarized neutron reflectivity (not shown) (sensitive to ferromagnetism) and diffraction (sensitive to the antiferromagnetism) have been performed at the Advanced Diffractometer for the Analysis of Materials (ADAM) at the Institut Laue-Langevin, Grenoble.³¹ Taking advantage of the large scattering angles available ($2\theta: 0-125^\circ$), we have accessed the half-order Bragg peak $(\frac{1}{2} \frac{1}{2} \frac{1}{2})$ and measured spin-analyzed reflection under the same conditions as low angle neutron reflectivity. The (111) Bragg peak was not accessible due to the large neutron wavelength ($\lambda = 4.41$ Å) available for this experiment.

A. Polarized neutron reflectivity study of the ferromagnetic layer

In Fig. 3 the magnetization reversal and the hysteresis loops are shown. The sample has been cooled from above the

Néel temperature of CoO ($T_N = 291$ K) to 10 K in an external magnetic field of 2 kOe to establish a unidirectional anisotropy. After field cooling in saturation, polarized neutron reflectivity curves were measured at 10 K to find the geometrical conditions (incident and outgoing angles) for maximum magnetic contrast²⁰ for the ferromagnetic layer. At this fixed geometry, spin-flip (SF) (I^{+-}, I^{-+}) and non-spin-flip (NSF) (I^{++}, I^{--}) reflected intensities were measured by sweeping the magnetic field. The SF intensities sense the magnetization component perpendicular to the applied field and scattering plane, whereas the NSF reflectivities are sensitive to the magnetization components parallel to the applied field. The field where the NSF reflected intensities are equal defines the coercive fields H_{c1} and H_{c2} , whereas the SF provides information on the magnetization reversal. We observe that on both sides of the hysteresis loop the remagnetization process of the ferromagnetic layer proceeds by domain wall movements. This is seen as vanishing SF intensities at the coercive fields. A rotation of the magnetization would lead to a strong increase in the SF reflectivity which is absent at both legs of the hysteresis loop. This contrasts with earlier observations, where an asymmetric reversal has been observed, albeit for a much thinner AF layer.^{16,20} Defining the spin asymmetry as $SA(B) = I^{++} - I^{--} / (I^{++} + I^{--} + I^{+-} + I^{-+})$, the normalized spin asymmetry $[SA(B) / SA(B_{sat})]$ allows us to measure a hysteresis loop. By measuring a second consecutive hysteresis loop, we observe that the system exhibits a small but clear training effect. The characteristics of the hysteresis loops are: (a) the magnetization reversal proceeds via domain nucleation and propagation for the first and all consecutive loops; (b) the exchange bias field is several orders of magnitude lower than predicted ($H_{EB} \approx 20$ Oe) and the coercive field is high $H_c \approx 650$ Oe. The exchange bias field is predicted to be $H_{EB} \approx 2000$ Oe, whereas the coercive field should not differ from the intrinsic

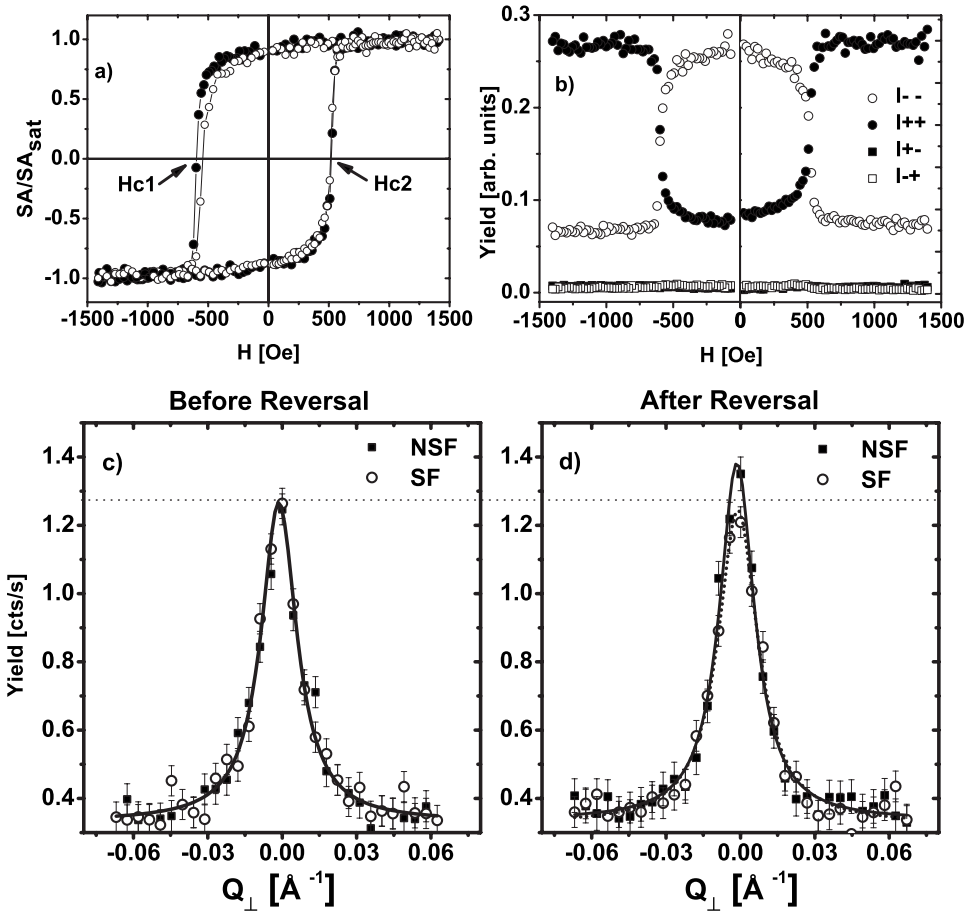


FIG. 3. The hysteresis loops (a) and the magnetization reversal (b) of the ferromagnetic layer. The NSF and SF scattering at the $(\frac{1}{2}\frac{1}{2}\frac{1}{2})$ antiferromagnetic half-order Bragg peak: (c) virgin state after field cooling from room temperature to 10 K and (d) the trained state after reversing once the magnetization. Both sets of data (c and d) are measured in an external field of 2 kOe.

value for the Py layer which is about 5 Oe (Refs. 2 and 9); (c) a small training effect is clearly seen by comparing two consecutive hysteresis loops shown in Fig. 3(a). Further hysteresis loops exhibit weaker relative changes (not shown).

Interestingly, the low value for the exchange bias is observed for epitaxial bilayers with very different thickness of the CoO layer, ranging from bulk CoO (Ref. 32) to nanometer thickness of the AF layer.^{6,25,33} Moreover, the absolute values of the exchange bias and coercive fields may be affected by the external field strength applied during cooling and during the hysteresis loop measurements.^{9,32}

B. Polarized neutron-diffraction study of the antiferromagnetic layer

Figures 3(c) and 3(d) show polarized neutron measurements which are sensitive only to the antiferromagnetic layer, taken after field cooling the sample from above T_N to 10 K, before and after reversing the magnetization. Spin-analyzed transverse scans were measured at the magnetic $(\frac{1}{2}\frac{1}{2}\frac{1}{2})$ reciprocal point [Fig. 3(c)]. We mention that a $\lambda/2$ contamination of the neutron beam can be excluded due to the vanishing intensity of the half-order peak above T_N [see Fig. 5(a)]. The transverse scans carry information about the average antiferromagnetic domain size and average orientation. The first observation is that after field cooling the NSF and SF cross sections are practically equal [see Fig. 3(c)]. This translates into almost equally populated $\{111\}$ domains

with a virtually anisotropic in-plane distribution of the AF spins. On average, an equal number of AF spins are oriented parallel and perpendicular to the ferromagnetic spins, respectively. We have calculated a lateral coherence length of ≈ 30 nm, in agreement with the resonant x-ray magnetic scattering results above [compare to Fig. 2(d)]. As a result, the cooling state of the Py/CoO system acquires a noncollinear magnetic state with a virtually anisotropic in-plane distribution of the AF domains, while the FM spins are aligned with the external field.

After reversing the magnetization at H_{c1} , the magnetic state of the AF layer may change as suggested indirectly by the magnetic interfacial roughness measured before¹³ leading to a training effect. By measuring the magnetic Bragg peak of the AF we access now directly the stability of the AF domain structure upon reversal. The spin-analyzed transverse scans shown in Fig. 3(d) were measured after a complete hysteresis loop. The external conditions for the scans before and after reversal are identical therefore, we may directly compare the virgin state of the AF layer after field cooling to the trained one. Surprisingly, after reversal the AF domain state does undergo irreversible changes. Under the influence of a strong direct interfacial coupling some domains appear to rearrange toward their stable configuration. The NSF intensity becomes stronger at the expense of SF scattering. This directly demonstrates that one origin of the training effect can be attributed to AF domain reorientation upon magnetization reversal.^{13,16,20} This AF domain instability further contributes to the spin-configurational relaxation³⁴ at the

F/AF interface. Moreover, our data provide clear evidence that the sharp decreasing component of the training effect originates from antiferromagnetic domains rearrangements during the very first magnetization reversals.

Now we describe an experiment (shown in Fig. 4) which can distinguish between an anisotropic in-plane AF spins orientations and a random AF spin orientational distribution. By anisotropic in-plane orientations we understand that the AF spins may be directed preferentially parallel to the anisotropy axes provided by the crystallographic axes, whereas a random orientational distribution of the AF spins would exhibit no preferential in-plane orientation. To this end we performed an azimuthal scan by measuring SF and NSF neutron integrated intensities at the $(\frac{1}{2}\frac{1}{2}\frac{1}{2})$ Bragg position while rotating the sample around its normal. Knowing that the scattering is a coherent process and that the SF probability is sensitive to the projection of the spin direction onto the SF axis but not to the absolute orientational angle, one would expect the normalized SF and NSF integrated intensities to be equal to

$$\frac{I^{\text{SF}}}{I^{\text{SF}} + I^{\text{NSF}}} = \left[\sum_0^{n-1} |\sin(\phi - \gamma * n)| \right]^2, \quad (1)$$

$$\frac{I^{\text{NSF}}}{I^{\text{SF}} + I^{\text{NSF}}} = 1 - \left[\sum_0^{n-1} |\sin(\phi - \gamma * n)| \right]^2,$$

where the integer $n = \pi/\gamma$ is the symmetry number, γ is the symmetry angle of the anisotropy axes, and ϕ is the azimuthal angle with $\phi=0$ defining the direction of an AF anisotropy axis. To obtain the equations above we also used a conservation law constraining the sum of the NSF and SF intensities to be constant as a function of the azimuthal angle. Assuming the AF spins to be oriented along the crystallographic (anisotropy) directions and making use of the structural data shown in Fig. 1(b), we extracted $\gamma = \pi/3$ and $n=3$. For this case, a SF and NSF integrated intensities modulation reflecting the sixfold structural symmetry should be observed. For the other case, of randomly in-plane oriented AF spins, the normalized SF and NSF yields should show a straight line as a function of the azimuthal angle. In Fig. 4 the experimental normalized SF and NSF integrated intensities are plotted as a function of the azimuthal angle (ϕ). The sample has been cooled down to 10 K in an external field of 2 kOe applied almost parallel to one of the AF anisotropy axes. The field was reversed as to induce the training effect. Then, the external field was reduced to about 50 Oe. We observe clear oscillations with a periodicity of 60° for both NSF and SF signals. The excellent agreement between the expected values [calculated by Eqs. (1) with $n=3$ and $\gamma = \pi/3$] based on the crystallographic data and the experimental observations in Fig. 4 leads us to the conclusion that the AF spins follow closely the anisotropy axes. They are not randomly oriented in plane. Previously, Scholl *et al.*³⁵ have also found orientational correlations between crystallographic and AF domains. In another publication by Nolting *et al.*³⁶ a one-to-one correspondence between the antiferromagnetic and ferromagnetic domains sizes as well as parallel

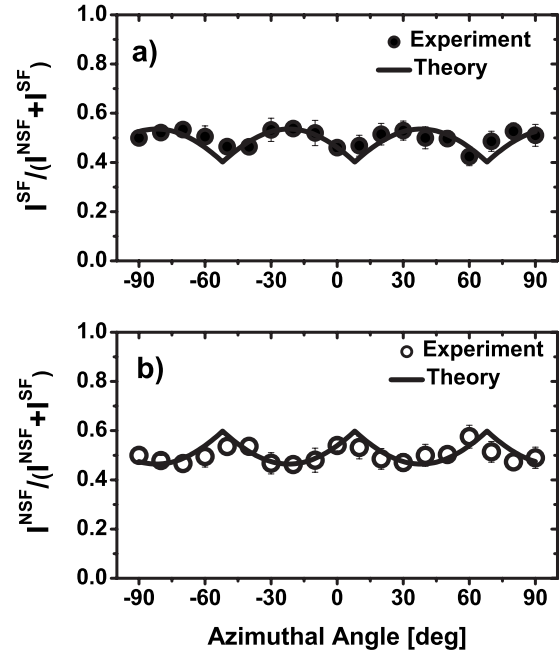


FIG. 4. Normalized (a) spin-flip $I^{\text{SF}}/(I^{\text{NSF}}+I^{\text{SF}})$ and (b) non-spin-flip $I^{\text{NSF}}/(I^{\text{NSF}}+I^{\text{SF}})$ $(\frac{1}{2}\frac{1}{2}\frac{1}{2})$ Bragg peak integrated intensities measured as a function of the azimuthal angle. The lines correspond to the theoretical expectations [calculated Eqs. (1) with $n=3$ and $\gamma = \pi/3$] when assuming a sixfold AF spin axes symmetry, in agreement with the structural data shown in Fig. 1(b). This graph shows that the AF spins are *not* randomly oriented in the film plane but aligned with the crystallographic axes.

coupling between the F and AF spins was observed. Here we find a fundamentally different situation, namely, that the ferromagnetic domains are much larger (as naturally expected in permalloy films) than the antiferromagnetic domains and the orientations of the AF spins are noncollinear with respect to the ferromagnetic spins.

These anisotropic orientations of the AF domains provide on average a virtually compensated interface and therefore, the exchange bias is several orders of magnitude lower than expected. Locally, each AF domain provides a bias projection along the cooling direction giving a large finite bias. In average, however, this large finite bias averages out due to anisotropic lateral orientations parallel to all crystallographic directions. The interfacial coupling of the local biasing appears in the hysteresis loop as strongly enhanced coercivity. An AF domain state is at the core of the domain state model.^{37–44} Their orientation is parallel to the anisotropy axis of the AF layer which has a unique direction. Here we observe experimentally more complex configurations of AF domains, with orientations distributed in plane and parallel to the three anisotropy axes. The spin glass (SG) model^{9,45} predicts a reduced AF anisotropy at the interface. This assumption may help to understand this particular domain state. Upon field cooling, the AF acquires its intrinsic domain state inside the film and by further cooling this configuration propagates toward the surface, minimizing the role of interfacial coupling.

To further confirm the influence of the AF domains on the exchange bias we have measured temperature-dependent AF

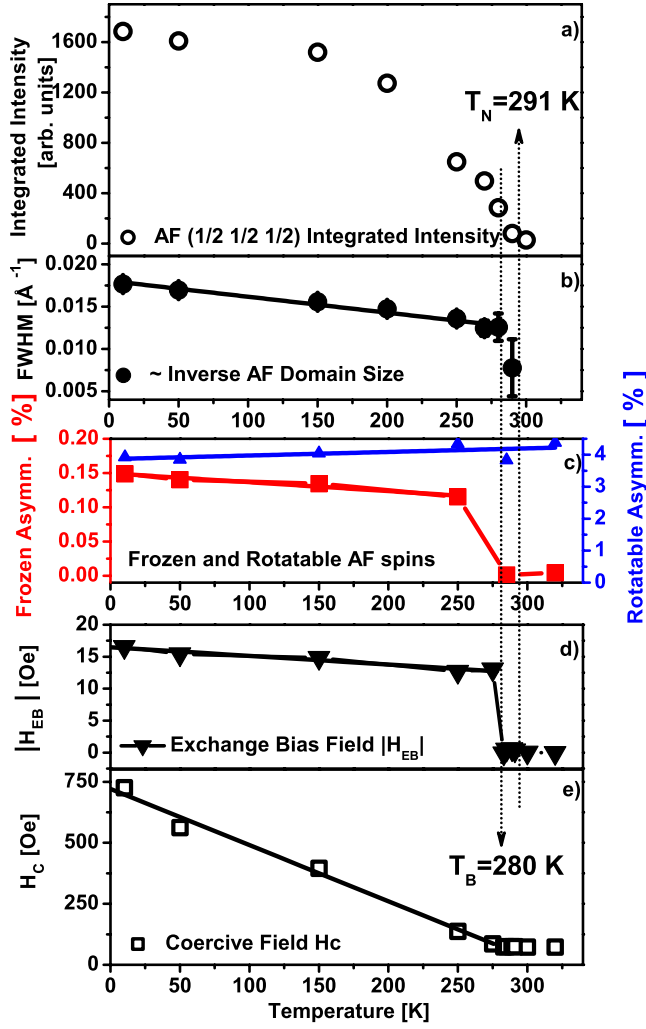


FIG. 5. (Color online) Temperature dependence of integrated intensity of the AF magnetic peak (a), in-plane AF coherence length (b), frozen-in and rotatable AF spins (c), and exchange bias (e) and coercive (d) fields.

Bragg peaks (not shown). They provide information on the antiferromagnetic order in a rather straightforward manner: above the Néel temperature the intensity of the half-order peak vanishes [see Fig. 5(a)], whereas at temperatures for which the long-range AF order is established it acquires non-vanishing values. The integrated peak intensity as a function of temperature provides the order parameter and the Néel temperature, which is 291 K for this sample, in agreement with earlier bulk measurements.⁴⁶ Moreover, the width of the AF peak shown in Fig. 5(b) contains additional information on the temperature dependence of the average AF domain size and the onset of their stability. The FWHM increases linearly as the temperature decreases, which translates into a smaller average domain size at low temperatures. The domain size evolution as function of temperature may be correlated with an increase in the wall width (grain boundary). This may be understood as an interplay between AF anisotropy and stiffness strengths. For instance, assuming random fields, Malozemoff model^{54–56} provides an analytical dependence for the characteristic length of the AF domains,

namely $L_{AF} \approx \sqrt{(A_{AF}/K_{AF})}$, where A_{AF} is the exchange stiffness and K_{AF} is the anisotropy of the antiferromagnet. Assuming that the anisotropy K_{AF} grows faster as compared to the exchange stiffness A_{AF} , one would expect a shrinking domain size when decreasing the temperature. The other situation, when A_{AF} grows faster as compared to K_{AF} , would lead to an increased AF domain size. Our experiments show a shrinking average domain size at low temperatures. This allows us to suggest that an anisotropy increase toward lower temperatures predominantly governs the average AF domain size. Another striking behavior is the observation of a characteristic temperature where the AF domains reach stability against the exchange interaction with the FM layer. This blocking temperature is $T_B = 280$ K and is lower than the Néel temperature. This correlates remarkably well with the blocking temperature for the exchange bias to be discussed further below. By contrast, the Néel temperature is the critical temperature which defines the onset of long-range spin order (against thermal fluctuations).

V. TEMPERATURE DEPENDENCE, FROZEN-IN UNCOMPENSATED SPINS, BLOCKING TEMPERATURE

Soft x-ray magnetic scattering measurements were performed at the UE46 HZB end station [Fig. 5(c)] and Alice diffractometer⁴⁷ [Figs. 5(d) and 5(e)] operated at the BESSY II PM3 bending magnet beamline. By tuning the energy close to the Co L_3 absorption edge, we have measured reflectivity curves which allow us to select the scattering conditions for maximum magnetic contrast.⁴⁸ In this way we measured element specific hysteresis loops as a function of temperature which yield the H_c and H_{EB} shown in Figs. 5(d) and 5(e), respectively. Flipping the circular helicity of x rays as well as the magnetic field allows us to separate rotatable and frozen-in AF spins⁹ which are depth and laterally uncompensated [Fig. 5(c)]. By contrast an ideal uncompensated monolayer assumed by the M&B model⁴⁹ is essentially depth and laterally compensated (see previous section) for our large AF layer, therefore it will not contribute to a shift of the macroscopic hysteresis loop. Sensitivity to monoatomic uncompensated M&B spins appears to be provided by a more localized probe like x-ray magnetic circular dichroism as debated in Refs. 50 and 51.

Measuring the reflected intensity for circularly right (I^{σ^+}) and left (I^{σ^-}) polarized x rays while sweeping the external field, one obtains a hysteresis loop provided by the asymmetry ratio as a function of an external field: $A(H) \equiv A = (I^{\sigma^+} - I^{\sigma^-}) / (I^{\sigma^+} + I^{\sigma^-})$. This asymmetry ratio resolves vertical shifts of the hysteresis loops, with respect to the magnetization axis. Now, the frozen-in and rotatable AF uncompensated components are extracted from the positive (A_{sat}^{pos}) and negative (A_{sat}^{neg}) magnetic saturation values of asymmetry as $A^F = (A_{sat}^{pos} + A_{sat}^{neg})/2$ and $A^R = (A_{sat}^{pos} - A_{sat}^{neg})/2$, respectively. These two experimental observables are plotted in Fig. 5(c) as a function of temperature. The sum of rotatable and frozen-in spins is seemingly constant (not shown) and extends through the Néel temperature.^{48,52,53} Note that the rotatable asymmetry component is much larger than the frozen asymmetry. At the blocking temperature, however, 3% of

these rotatable AF spins become frozen with a sharp characteristic onset. Note that the absolute asymmetry values for the frozen-in spins [Fig. 5(c)] are below 0.0015, which reflects an exceptionally high precision (not achieved before) for these measurements. At lower temperatures a linear increase in the frozen-in asymmetry is clearly observed and correlates with the in-plane AF coherence length. The direct relation between the size of AF domains and the uncompensated spins is intrinsic to the Malozemoff model.^{54–56} Calculating the H_{EB} for this system within the Malozemoff model⁹ one would expect it to be about 600 Oe. The measured H_{EB} value of about 20 Oe is still 30 times lower.

H_c increases linearly as a function of temperature, confirming a strong interfacial coupling. The exchange bias shows, however, a very different behavior. After a sharp onset at the blocking temperature ($T_B=280$ K), it increases linearly toward low temperatures. The blocking temperature can be correlated with the temperature where the AF domains achieve stability against the exchange interaction with the FM layer as observed by neutron scattering [Fig. 5(b)]. This origin of the blocking temperature can be inferred from the M&B model. There, the blocking temperature is always lower than the Néel temperature and is essentially governed by the magnitude of the AF anisotropy energy and interfacial exchange energy. The temperature where the AF (effective) anisotropy becomes strong enough to resist the rotation (remagnetization) of the ferromagnetic spins is defined as blocking temperature.^{9,49}

The astounding correlations between the temperature evolution of the AF domain size, frozen-in spins, and value of exchange bias are shown in Fig. 5. The temperature dependence of the H_{EB} and of frozen-in spins is correlated with the average AF domain size and orientation. Characteristic features of three different models can be inferred from these data: the origin of the blocking temperature can be described by the M&B model, the formation of AF domains is intrinsic

to the DS and Malozemoff models, and the linear dependence between the AF frozen spins and the AF domain sizes is characteristic to the Malozemoff model, demonstrating their limitations. These features, including the noncollinearity between the AF and FM spins, can all be accounted for by the SG model.^{9,45}

VI. CONCLUSIONS

In conclusion, we have investigated an archetypal exchange bias bilayer by using complementary neutron and x-ray diffraction techniques. An almost anisotropic orientation of AF domains is observed, thus, clarifying the origin of the reduction in the exchange bias field in epitaxially grown CoO/FM bilayers by several orders of magnitude. The blocking temperature for the exchange bias is the temperature where the antiferromagnetic domains achieve stability against the exchange interaction with the FM layer. By contrast, at the Néel temperature the AF system develops a long-range order against thermal fluctuations. At low temperatures, the antiferromagnetic domains are not stable upon magnetization reversal, which is directly identified as one contribution to the training effect. Uncompensated frozen-in spins are found to be remarkably well correlated with the antiferromagnetic domains and the exchange bias field. This strongly supports a mechanism for exchange bias caused by interfacial uncompensated spins.

ACKNOWLEDGMENTS

We gratefully acknowledge the excellent support provided by T. Kachel and R. Follath during the measurements. The ALICE diffractometer is funded through the BMBF Contract No. 05KS7PC1. The ADAM instrument is funded through the BMBF Contract No. 03ZA7BOC.

*Florin.Radu@helmholtz-berlin.de

¹S. A. McEnroe, B. Carter-Stiglitz, R. J. Harrison, P. Robinson, K. Fabian, and C. McCammon, *Nat. Nanotechnol.* **2**, 631 (2007).

²W. H. Meiklejohn and C. P. Bean, *Phys. Rev.* **102**, 1413 (1956).

³M. N. Baibich, J. M. Broto, A. Fert, F. Nguyen Van Dau, F. Petroff, P. Eitenne, G. Creuzet, A. Friederich, and J. Chazelas, *Phys. Rev. Lett.* **61**, 2472 (1988).

⁴G. Binasch, P. Grünberg, F. Saurenbach, and W. Zinn, *Phys. Rev. B* **39**, 4828 (1989).

⁵A. E. Berkowitz and K. Takano, *J. Magn. Magn. Mater.* **200**, 552 (1999).

⁶J. Nogues and I. K. Schuller, *J. Magn. Magn. Mater.* **192**, 203 (1999).

⁷R. L. Stamps, *J. Phys. D* **33**, R247 (2000).

⁸M. Kiwi, *J. Magn. Magn. Mater.* **234**, 584 (2001).

⁹F. Radu and H. Zabel, *Springer Tracts Mod. Phys.* **227**, 97 (2008).

¹⁰O. Iglesias, A. Labarta, and X. Batlle, *J. Nanosci. Nanotechnol.* **8**, 2761 (2008).

¹¹V. I. Nikitenko, V. S. Gornakov, A. J. Shapiro, R. D. Shull, K.

Liu, S. M. Zhou, and C. L. Chien, *Phys. Rev. Lett.* **84**, 765 (2000).

¹²M. R. Fitzsimmons, P. Yashar, C. Leighton, I. K. Schuller, J. Nogues, C. F. Majkrzak, and J. A. Dura, *Phys. Rev. Lett.* **84**, 3986 (2000).

¹³F. Radu, M. Etzkorn, T. Schmitte, R. Siebrecht, A. Schreyer, K. Westerholt, and H. Zabel, *J. Magn. Magn. Mater.* **240**, 251 (2002).

¹⁴W.-T. Lee, S. G. E. te Velthuis, G. P. Felcher, F. Klose, T. Gredig, and E. D. Dahlberg, *Phys. Rev. B* **65**, 224417 (2002).

¹⁵M. Gierlings, M. J. Prandolini, H. Fritzsche, M. Gruyters, and D. Riegel, *Phys. Rev. B* **65**, 092407 (2002).

¹⁶S. Brems, D. Buntinx, K. Temst, C. Van Haesendonck, F. Radu, and H. Zabel, *Phys. Rev. Lett.* **95**, 157202 (2005).

¹⁷D. Paccard, C. Schlenker, O. Massenet, R. Montmory, and A. Yelon, *Phys. Status Solidi* **16**, 301 (1966).

¹⁸J. Nogues, D. Lederman, T. J. Moran, and I. K. Schuller, *Phys. Rev. Lett.* **76**, 4624 (1996).

¹⁹T. M. Hong, *Phys. Rev. B* **58**, 97 (1998).

²⁰F. Radu, M. Etzkorn, R. Siebrecht, T. Schmitte, K. Westerholt,

- and H. Zabel, *Phys. Rev. B* **67**, 134409 (2003).
- ²¹T. Gredig, I. N. Krivorotov, P. Eames, and D. Dahlberg, *Appl. Phys. Lett.* **81**, 1270 (2002).
 - ²²M. Ali, P. Adie, C. H. Marrows, D. Greig, B. J. Hickey, and R. L. Stamps, *Nature Mater.* **6**, 70 (2007).
 - ²³E. Dudzik, R. Feyerherm, R. Signorato, and C. Zilkens, *J. Synchrotron Radiat.* **13**, 421 (2006).
 - ²⁴A. Erko, I. Packe, C. Hellwig, M. Fieber-Erdmann, O. Pawlitzki, M. Veldkamp, and W. Gudat, *Proceedings of the 11th US National Conference on Synchrotron Radiation Instrumentation, SRI99*, AIP Conf. Proc. No. 521 (AIP, New York, 2000), p. 415.
 - ²⁵G. Nowak, A. Remhof, F. Radu, A. Nefedov, H.-W. Becker, and H. Zabel, *Phys. Rev. B* **75**, 174405 (2007).
 - ²⁶N. J. Gökemeijer, R. L. Penn, D. R. Veblen, and C. L. Chien, *Phys. Rev. B* **63**, 174422 (2001).
 - ²⁷Z. Nishiyama, *Sci. Rep. Tohoku Imp. Univ., Ser. 1* **23**, 638 (1934).
 - ²⁸J. A. Borchers, R. W. Erwin, S. D. Berry, D. M. Lind, J. F. Ankner, E. Lochner, K. A. Shaw, and D. Hilton, *Phys. Rev. B* **51**, 8276 (1995).
 - ²⁹H. Béa, M. Bibes, F. Ott, B. Dupe, X.-H. Zhu, S. Petit, S. Fusil, C. Deranlot, K. Bouzehouane, and A. Barthelemy, *Phys. Rev. Lett.* **100**, 017204 (2008).
 - ³⁰S. I. Csizar, Ph.D. thesis, University of Groningen, the Netherlands, 2005.
 - ³¹M. Wolff, K. Zhernenkov, and H. Zabel, *Thin Solid Films* **515**, 5712 (2007).
 - ³²T. J. Moran and I. K. Schuller, *J. Appl. Phys.* **79**, 5109 (1996).
 - ³³K. Takano, R. H. Kodama, A. E. Berkowitz, W. Cao, and G. Thomas, *Phys. Rev. Lett.* **79**, 1130 (1997).
 - ³⁴C. Binek, *Phys. Rev. B* **70**, 014421 (2004).
 - ³⁵A. Scholl, J. Stöhr, J. Lüning, J. W. Seo, J. Fompeyrine, H. Siegwart, J. P. Locquet, F. Nolting, S. Anders, E. E. Fullerton, M. R. Scheinfein, and H. A. Padmore, *Science* **287**, 1014 (2000).
 - ³⁶F. Nolting, A. Scholl, J. Stöhr, J. W. Seo, J. Fompeyrine, H. Siegwart, J. P. Locquet, S. Anders, J. Lüning, E. E. Fullerton, M. F. Toney, M. R. Scheinfein, and H. A. Padmore, *Nature (London)* **405**, 767 (2000).
 - ³⁷P. Miltényi, M. Gierlings, J. Keller, B. Beschoten, G. Güntherodt, U. Nowak, and K. D. Usadel, *Phys. Rev. Lett.* **84**, 4224 (2000).
 - ³⁸U. Nowak, A. Misra, and K. D. Usadel, *J. Appl. Phys.* **89**, 7269 (2001).
 - ³⁹U. Nowak, A. Misra, and K. D. Usadel, *J. Magn. Magn. Mater.* **240**, 243 (2002).
 - ⁴⁰U. Nowak, K. D. Usadel, J. Keller, P. Miltényi, B. Beschoten, and G. Güntherodt, *Phys. Rev. B* **66**, 014430 (2002).
 - ⁴¹B. Beckmann, U. Nowak, and K. D. Usadel, *Phys. Rev. Lett.* **91**, 187201 (2003).
 - ⁴²A. Misra, U. Nowak, and K. D. Usadel, *J. Appl. Phys.* **95**, 1357 (2004).
 - ⁴³G. Scholten, K. D. Usadel, and U. Nowak, *Phys. Rev. B* **71**, 064413 (2005).
 - ⁴⁴B. Beckmann, K. D. Usadel, and U. Nowak, *Phys. Rev. B* **74**, 054431 (2006).
 - ⁴⁵F. Radu, A. Westphalen, K. Theis-Bröhl, and H. Zabel, *J. Phys.: Condens. Matter* **18**, L29 (2006).
 - ⁴⁶W. L. Roth, *Phys. Rev.* **110**, 1333 (1958).
 - ⁴⁷J. Grabis, A. Nefedov, and H. Zabel, *Rev. Sci. Instrum.* **74**, 4048 (2003).
 - ⁴⁸F. Radu, A. Nefedov, J. Grabis, G. Nowak, A. Bergmann, and H. Zabel, *J. Magn. Magn. Mater.* **300**, 206 (2006).
 - ⁴⁹W. H. Meiklejohn and C. P. Bean, *Phys. Rev.* **105**, 904 (1957).
 - ⁵⁰H. Ohldag, T. J. Regan, J. Stöhr, A. Scholl, F. Nolting, J. Lüning, C. Stamm, S. Anders, and R. L. White, *Phys. Rev. Lett.* **87**, 247201 (2001).
 - ⁵¹M. Tsunoda, T. Nakamura, M. Naka, S. Yoshitaki, C. Mitsumata, and M. Takahashi, *Appl. Phys. Lett.* **89**, 172501 (2006).
 - ⁵²S. Roy, C. Sanchez-Hanke, S. Park, M. R. Fitzsimmons, Y. J. Tang, J. I. Hong, D. J. Smith, B. J. Taylor, X. Liu, M. B. Maple, A. E. Berkowitz, C.-C. Kao, and S. K. Sinha, *Phys. Rev. B* **75**, 014442 (2007).
 - ⁵³R. Abrudan, J. Miguel, M. Bernien, C. Tieg, M. Piantek, J. Kirschner, and W. Kuch, *Phys. Rev. B* **77**, 014411 (2008).
 - ⁵⁴A. P. Malozemoff, *Phys. Rev. B* **35**, 3679 (1987).
 - ⁵⁵A. P. Malozemoff, *J. Appl. Phys.* **63**, 3874 (1988).
 - ⁵⁶A. P. Malozemoff, *Phys. Rev. B* **37**, 7673 (1988).